analytical chemistry

Article

pubs.acs.org/ac

Magnetic Zirconium Hexacyanoferrate(II) Nanoparticle as Tracing Tag for Electrochemical DNA Assay

Guang-Yao Zhang,[†] Sheng-Yuan Deng,[†] Wen-Rong Cai,[†] Serge Cosnier,[‡] Xue-Ji Zhang,[†] and Dan Shan*[,†]

[†]School of Environmental and Biological Engineering, Nanjing University of Science and Technology, Nanjing, Jiangsu 210094, China

[‡]University of Grenoble Alpes-CNRS, DCM UMR 5250, F-38000 Grenoble, France

Supporting Information

ABSTRACT: Novel multifunctional magnetic zirconium hexacyanoferrate nanoparticles (ZrHCF MNPs) were prepared, which consisted of magnetic beads (MBs) inner core and zirconium hexacyanoferrate(II) (ZrHCF) outer shell. As an artificial peroxidase, the ZrHCF MNPs exhibited remarkable electrocatalytic properties in the reduction of H_2O_2 at 0.2 V vs saturated calomel electrode (SCE). On the basis of the bonding interaction between Zr (IV) of the shell ZrHCF framework and phosphonate groups, the 5′-phosphorylated ssDNA probes with a consecutive stretch of guanines as a spacer could be incorporated in ZrHCF MNPs easily. Thus, DNA-grafted ZrHCF MNPs could be simply obtained by magnetic separation. The prepared nanoelectrocatalyst was further used as signal nanoprobe for the ultrasensitive electrochemical DNA assay. Under optimal conditions, the proposed biosensor presents high sensitivity for detecting target DNA with a linear range from 1.0 fM to 1.0 nM and a low detection limit of 0.43 fM. Moreover, it exhibits good performance with excellent selectivity, high stability, and acceptable fabrication reproducibility.

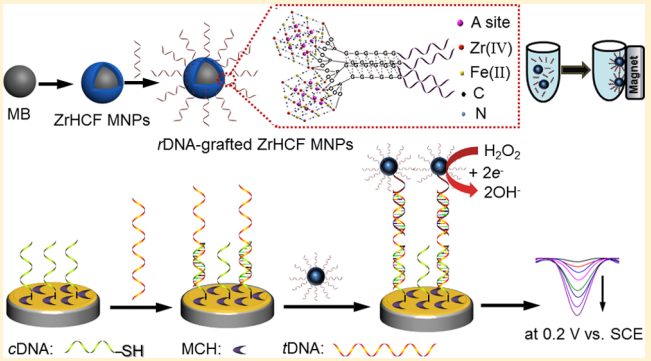

The ultrasensitive detection of DNA provides potential application in the fields of clinical diagnosis, biological research, environmental monitoring, and food safety.[1−4] Among these detection methods for nucleic acid, an electrochemical sensor attracts much more attention on account of their high sensitivity, portability, simplicity, low cost, and reusablility.[5−8] In order to realize an ultrasensitive bioassay, the conventional strategies of DNA biosensors often rely on bioengineered enzyme-linked probes, generating detection signal by the catalytic substrate reaction.[9,10] However, enzyme-based bioassays often suffer from shortcomings associated with the limited stability and cost of natural enzymes. Hence, the stable nonenzymatic nanoelectrocatalysts with high catalytic efficiencies are highly desirable for the DNA bioassay.

Magnetic beads (MBs) have widespread biomedical applications because of their unique property: superparamagnetism.[11] They are often used to enrich, separate, and immobilize DNA or proteins.[12−15] However, for the biosensing, the biological functional treatments of MBs are often necessary.[16] Some biomaterial-functionalized MBs, such as thionine-doped magnetic gold nanospheres and Fe_3O_4@Ag−Pd hybrid nanoparticles, have been extensively applied in the electrochemical bioassay.[17,18] Among them, the Prussian blue (PB) modified MBs have become quite attractive due to their advantages: (1) PB or PB analogy nanoparticles can be employed as an artificial peroxidase because of their high electrocatalytic activity toward H_2O_2 reduction at low overpotential;[19] (2) PB exhibits excellent electrochemical behavior to promote the heterogeneous electron transfer.[20] Above all, the nanocomposites can show both superparamagnetism and peroxidase-like activity.

On the other hand, the unique coordination of phosphate groups to metal(IV), such as Zr (IV) and Ti (IV), has been shown in extensive applications, including self-assembled monolayers,[21,22] protein microarrays,[23] DNA microarrays,[24] phosphopeptide enrichment,[25] and bioassay.[26,27] Recently, Zr-based nanomaterials, such as zirconium oxide (ZrO_2) and Zr-based metal−organic frameworks (MOFs), have been applied to the selective enrichment of phosphopeptides[28−30] and the immobilization of DNA probe[31] based on the coordination binding zirconium to phosphate groups of biomolecules.

In this work, zirconium hexacyanoferrate nanoparticles were loaded on the surface of amino-functionalized Fe_3O_4 magnetic beads (MBs) to form novel magnetic core−shell zirconium hexacyanoferrate nanoparticles (ZrHCF MNPs). Zr (IV) on the shell ZrHCF framework may provide a valid binding site for DNA via phosphate groups. The single-stranded DNA can be firmly assembled on the ZrHCF MNPs by the "zirconium−(OPO_3-poly(dG) DNA)" covalent bonds to maintain DNA 5′

Received: June 26, 2015
Accepted: August 10, 2015

DOI: 10.1021/acs.analchem.5b02395
Anal. Chem. XXXX, XXX, XXX−XXX

Scheme 1. (A) Preparation Procedures of *r*DNA-Grafted ZrHCF MNPs. (B) Schematic Illustration of the Stepwise DNA Assay Construction Process

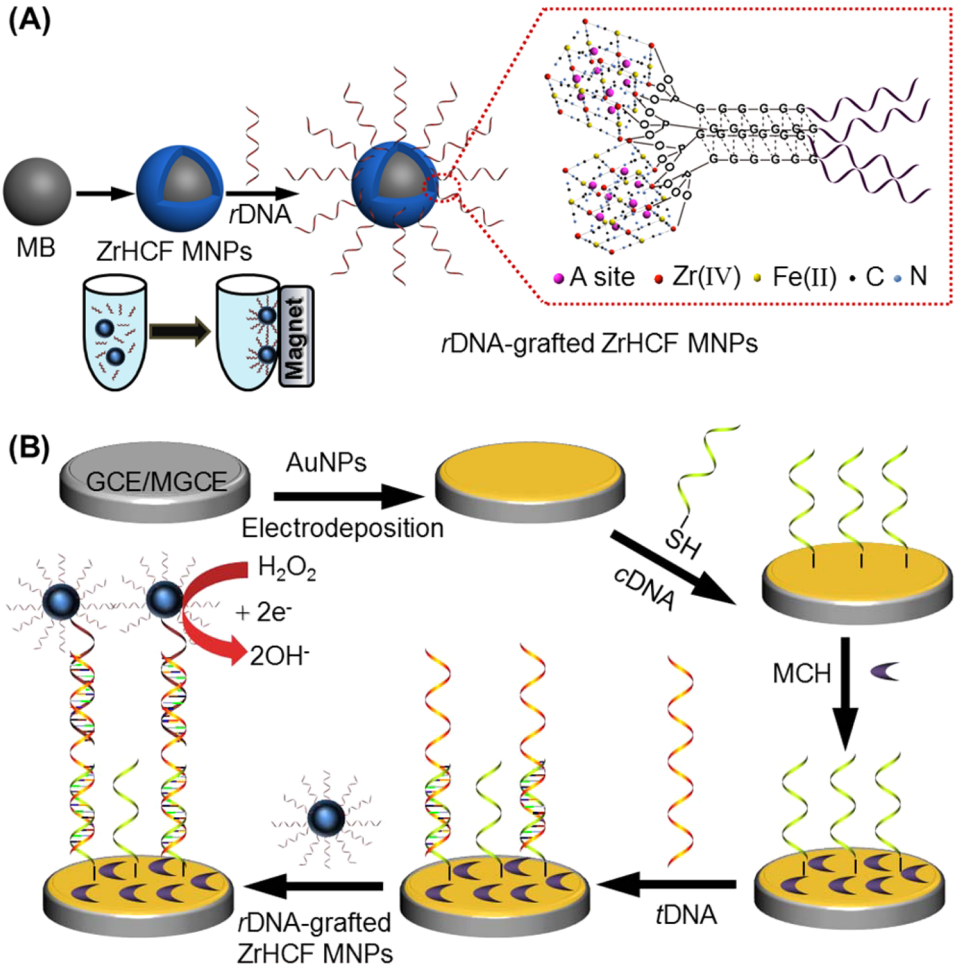

terminal-orientation. Thus, DNA-grafted ZrHCF MNPs could be simply obtained by magnetic separation, instead of the complicated chemical modification for the functional groups in the terminal DNA. It may also provide an efficient signal transduction platform for the ultrasensitive detection of DNA. This ZrHCF MNPs-based strategy opens up a promising area for the determination of various analytes for signal transduction in bioanalytical applications.

EXPERIMENTAL SECTION

Materials and Reagents. Chloroauricacid trihydrate ($HAuCl_4 \cdot 3H_2O$, CAS: 27988-77-8), potassium hexacyanoferrate(III) ($K_3Fe(CN)_6$, CAS: 13746-66-2), zirconyl chloride ($ZrOCl_2$, CAS: 7699-43-6) solution (30% in hydrochloric acid (HCl)), dopamine hydrochloride (CAS: 62-31-7), and 6-mercapto-1-hexanol (MCH, 97%, CAS: 1633-78-9) were purchased from the local Sigma−Aldrich Chemical Co. (Shanghai, China). Iron oxide (Fe_3O_4) superparamagnetic microbeads (MBs, 5 mg mL^{-1}, ~100 nm in diameter) with amine ($-NH_2$) stabilizers in an aqueous suspension were obtained from Tianjin BaseLine Chromtech Research Centre (Tianjin, China). Hydrogen peroxide (H_2O_2, 30 wt %, CAS: 7722-84-1) solution was purchased from Sinopharm Chemical Reagent Co., Ltd. (Beijing, China). All other reagents were of analytical grade and were used without further purification. Ultrapure water obtained from a Millipore water purification system (≥18 MΩ, Milli-Q, Millipore) was used in all assays. Human serum samples were provided by Jiangsu Province Tumor Hospital.

The oligonucleotides were synthesized and purified via high-performance liquid chromatography (HPLC) by Shanghai Sangon Biotechnology Co., Ltd. (Shanghai, China) with sequences listed as follows:

Capture DNA (*c*DNA): 5′−CCTATCTACCATGCT−$(CH_2)_6$−SH−3′

Target DNA (*t*DNA):

5′−AGCATGGTAGATAGGTTTTTTTATAGGACTCTGGCGC−3′

Single-base mismatched DNA (*sm*DNA):

5′−AGCATGGTCGATAGGTTTTTTTATAGGACTCTGGCGC−3′

Three-base mismatched DNA (*tm*DNA):

5′−AGCATGGTCGATATGTTTTTTTTATAGGAATCTGGCGC−3′

Reporter DNA1 (*r*DNA1): 5′−GGGGGGTTGCGCCAGAGTCCTAT−3′

Reporter DNA2 (*r*DNA2): 5′−ACATCATTGCGCCAGAGTCCTAT−3′

TE buffer (10 mM Tris-HCl, containing 1 mM EDTA and 0.3 M NaCl, pH 7.9) was used for dissolving these oligonucleotides.

DOI: 10.1021/acs.analchem.5b02395
Anal. Chem. XXXX, XXX, XXX−XXX

Apparatus. A CHI 660D electrochemical workstation (CHI Co., USA) was used for cyclic voltammetry (CV) and differential pulse voltammetric (DPV) measurements. Electrochemical impedance spectroscopy (EIS) measurements were carried out using an Autolab PGSTAT30 (Eco chemie, The Netherlands) controlled by NOVA 1.10 software. The EIS measurements were performed in 5 mM $[Fe(CN)_6]^{3-/4-}$ containing 0.1 M KCl. The amplitude of the applied sine wave potential was 5 mV. The impedance measurements were recorded at a bias potential of 190 mV within the frequency range of 0.1 Hz to 10 kHz. All electrochemical studies were performed with a conventional three electrode system. A saturated calomel electrode (SCE) and a Pt wire electrode were used as reference and counter electrodes, respectively. All the potentials mentioned below are relative to SCE. Bare and modified glassy carbon (GCE, 3 mm in diameter) or magnetic glassy carbon electrode (MGCE, 3 mm in diameter) were used as working electrodes. The morphology of the as-synthesized nanomaterials was investigated with a XL-30E scanning electron microscope (SEM). The X-ray photoelectron spectroscopy (XPS) experiments were carried out on K-Alpha (Thermo Fisher Scientific Co., USA). The Gaussian−Lorentzian distribution was used for fitting the spectra for each peak, in order to determine the binding energy of the core levels of the different elements. Fourier transform infrared (FT-IR) spectra were measured on a pressed KBr pellet employing a TENSOR Model 27 FT-IR spectrometer.

Preparation of ZrHCF. ZrHCF naoparticles were prepared according to the reported method.[32] Briefly, $K_3Fe(CN)_6$, $ZrOCl_2$, and dopamine were dissolved in 10 mM HCl aqueous solution, respectively. 1.0 mL of 10 mM $K_3Fe(CN)_6$, 1 mL of 10 mM $ZrOCl_2$, and 1 mL of 1 mM dopamine were added in succession under vigorous stirring for 1 h. An ivory-white precipitate formed immediately. The precipitate was washed with double-distilled water for three times by centrifugation to obtain ZrHCF nanoparticles and stored at 4 °C before use.

Preparation of ZrHCF MNPs. MBs were initially washed for several times with double-distilled water in the presence of the external magnet; then, they were diluted into 1 mg mL^{-1} with 10 mM HCl and applied as seeds for the generation of ZrHCF, which was followed by adding dropwise 1 mL of 10 mM $K_3Fe(CN)_6$ containing 10 mM HCl and subsequent stirring for 30 min. Afterward, 1 mL of $ZrOCl_2$ and 1 mL of 1 mM dopamine (both containing 10 mM HCl) were introduced successively and stirred for 1 h. The obtained ZrHCF MNPs were washed thoroughly with 10 mM HCl by magnetic separation with repeated decantation of the supernatant until colorless. Finally, the collected ZrHCF MNPs were rinsed and neutralized with double-distilled water and stored at 4 °C prior to use.

Preparation of *r*DNA-Grafted ZrHCF MNPs. The protocol for *r*DNA-grafted ZrHCF MNPs preparation is illustrated in Scheme 1A. First, the as-synthesized ZrHCF MNPs were redispersed into 1 mL of ultrapure water and incubated with 100 μL of *r*DNA (10 μM) for 12 h at room temperature. Unconjugated *r*DNA was removed magnetically, and the obtained nanocomposite was redispersed in 1 mL of ultrapure water before its stepwise application.

Fabrication of the DNA Biosensor. The fabrication procedure of the DNA biosensor is illustrated in Scheme 1B. First, GCE was polished with 0.3 and 0.05 μm of alumina slurry, respectively, and sonicated sequentially in absolute ethanol and double-distilled water before access to a mirror-like surface. The pretreated electrode was immersed in $HAuCl_4$ solution for the electrodeposition of a nanogold layer at a potential of −0.2 V for 20 s. Second, 10 μL of 2 μM *c*DNA was pipetted onto the gold nanoparticles-modified GCE for 16 h at room temperature. The electrode surface was subjected to stream rinsing and blocking the unspecific sites with 1.0 mM MCH for 1 h. Third, 10 μL of *t*DNA with different concentrations was casted onto the electrode and incubated at 37 °C for 2 h. Subsequently, the as-prepared DNA sensor was incubated with 10 μL of *r*DNA-grafted ZrHCF MNPs at 37 °C for 90 min. After rinsing, the electrode would generate electrochemical signal from the H_2O_2 reduction by ZrHCF MNPs and gave the quantitative criteria for the proposed DNA assay.

RESULTS AND DISCUSSION

Characterization of the MBs, ZrHCF, and ZrHCF MNPs. The morphologies of the as-prepared MBs and ZrHCF MNPs were investigated by SEM (Figure 1). The MBs are near-

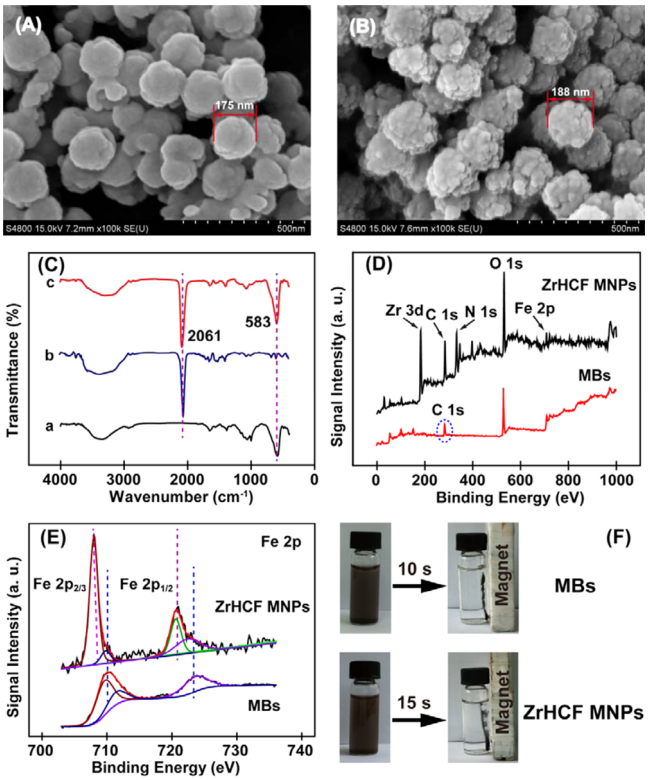

Figure 1. SEM images of (A) MBs and (B) ZrHCF MNPs. (C) FT-IR spectra of MBs (a), ZrHCF (b), and ZrHCF MNPs (c). The XPS survey scans (D) and the high-resolution XPS response of Fe 2p (E) core energy levels for ZrHCF MNPs and MBs. (F) Easy separation of MBs and ZrHCF MNPs by commercial magnet.

spherical with a relatively smooth surface (Figure 1A), and the particle size is about 175 nm. In the process of the ZrHCF MNPs formation, first, the negatively charged ferricyanide ion $(Fe(CN)_6^{3-})$ would be electrostatically adsorbed on their surface due to the protonation of amines on the surface of MBs. Second, dopamine can convert $Fe(CN)_6^{3-}$ into its reduced form $Fe(CN)_6^{4-}$. The latter would further react with Zr (IV), resulting in the ZrHCF precipitates. Obviously, the obtained ZrHCF MNPs have a quite rough surface similar to the cauliflower shape (Figure 1B), and the particle size is larger

DOI: 10.1021/acs.analchem.5b02395
Anal. Chem. XXXX, XXX, XXX−XXX

about 188 nm, respectively. It implies the ZrHCF MNPs have a core−shell heterostructure with the core MBs and the shell ZrHCF precipitates. The comparison of the as-prepared MBs, ZrHCF, and ZrHCF MNPs is further given by FT-IR. As shown in Figure 1C, the IR spectrum of ZrHCF MNPs exhibits a distinguished band at 2061 cm^{-1} attributed to the cyanide groups coordinated to transition metals (Fe^{II}−CN−Zr^{IV}),[33,34] and an absorption band at 583 cm^{-1} is assigned to the Fe═O stretching mode of the bulk Fe_3O_4 MBs,[35] indicating the presence of the ZrHCF frame on the surface of the MBs.

Moreover, the XPS survey scans of the surface for the ZrHCF MNPs and MBs in the range of 0−1000 eV are presented in Figure 1D. The C, O, and Fe elements can be clearly observed in the two nanomaterials. The carbon in the MBs is attributed to the carbon polymer around the MBs. In addition, the Zr 3d and N 1s are extremely visible in the ZrHCF MNPs corresponding to the ZrHCF nanoparticles coating on the surface of MBs. In contrast, the main differences between the MBs and ZrHCF MNPs are demonstrated in the XPS spectra of Fe 2p (Figure 1E) and N 1s (Figure S1), respectively. For the ZrHCF MNPs, the Fe 2p spectrum shows four main peaks at 708.0 and 710.1 (Fe $2p_{2/3}$) and 720.6 and 722.5 eV (Fe $2p_{1/2}$) using the curve fitting procedure. The binding energies, 708.0 and 720.6 eV, were due to Fe (II) in the ZrHCF formation.[36] On the other hand, the other two peaks come from the MBs, and the broad peak at around 710.1 eV may be deconvoluted into two components at 709.9 and 711.8 eV, assigned to Fe (II) and Fe (III) from the formation of Fe_3O_4, respectively.[37] Similarly, the N 1s spectrum contains two peaks at 397.0 and 398.6 eV in ZrHCF MNPs (Figure S1). The presence of N 1s at 397.0 eV originated from the cyanide groups of the ZrHCF formation, and the peak at 398.6 eV obtained for ZrHCF MNPs can be attributed to the amine groups functional MBs. However, the peak at 399.9 eV is present from the amino groups in the MBs; the peak position shift may be caused by the interaction between the amine groups functional MBs and the shell ZrHCF nanoparticles. Meanwhile, The MBs and ZrHCF MNPs can be quickly separated by a commercial magnet, demonstrating ZrHCF MNPs also possess favorable superparamagnetic properties (Figure 1F).

Afterward, Figure 2A shows the XPS survey scans of the surface for the *r*DNA-grafted ZrHCF MNPs in the range of 0−1000 eV. Apart from the C, N, O, Fe, and Zr elements shown, the P 2p peak at 132.7 eV is perceived because of phosphate groups from DNA (Figure 2B). At the same time, the difference of the Zr 3d spectrum between the ZrHCF MNPs and *r*DNA-grafted ZrHCF MNPs is investigated by XPS (Figure 2C,D). In the XPS spectrum for the ZrHCF MNPs, the Zr 3d exhibits two main peaks at 181.8 and 184.1 eV (Figure 2C). These two peaks are also curve-fitting obtained in the Zr 3d spectrum for the *r*DNA-grafted ZrHCF MNPs (Figure 2D). In addition, two components centered at 181.0 and 183.4 eV are gained by the decomposition procedure, corresponding to Zr−O−P from the coordination of the ZrHCF MNPs and DNA. These results suggest that the *r*DNA-grafted ZrHCF MNPs can be availably formed by simple magnetic separation.

PB or PB analogy nanoparticles, as an artificial peroxidase, have shown effective application value in the field of biological analysis.[38−40] Meanwhile, utilizing the ability of the ZrHCF MNPs to enrich and separate DNA in the magnetic field, we may develop a simple DNA biosensor.

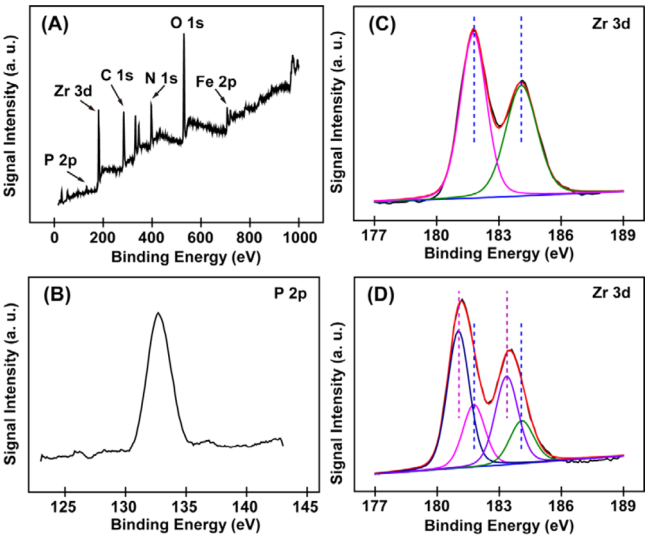

Figure 2. XPS survey scans (A) and the high-resolution XPS response of P 2p (B) core energy levels for *r*DNA-grafted ZrHCF MNPs. The high-resolution XPS response of Zr 3d core energy levels for ZrHCF MNPs (C) and *r*DNA-grafted ZrHCF MNPs (D).

Characterization of the DNA Biosensor. The self-assembled process of the proposed biosensor was further investigated by CV and EIS. Figure 3A displays the CV curves

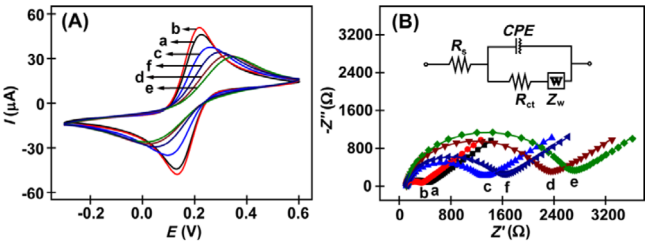

Figure 3. (A) CVs and (B) EIS for each immobilized step in 5 mM $Fe(CN)_6^{4-/3-}$ solution containing 0.1 M KCl: (a) bare GCE, (b) GCE/AuNPs, (c) GCE/AuNPs/*c*DNA, (d) GCE/AuNPs/*c*DNA/MCH, (e) GCE/AuNPs/*c*DNA/MCH/ *t*DNA, and (f) GCE/AuNPs/*c*DNA/MCH/*t*DNA/*r*DNA-grafted ZrHCF MNPs (scan rate of 50 mV s^{-1}, impedance spectral frequency of 0.1−10^5 Hz, amplitude of 5 mV); points are experimental data, and solid lines are fitted curves. Inset B: Equivalent circuit.

of the modified GCE at different stages using $Fe(CN)_6^{4-/3-}$ as a sensitive redox probe. Clearly, the bare GCE exhibited a couple of reversible redox peaks (curve a). After AuNPs were electrodeposited onto the surface of electrode, the peak current apparently increased (curve b). The increasing response is attributed to the excellent electrical conductivity of AuNPs. When the *c*DNA was immobilized onto the above modified electrode, the peak current decreased dramatically and the peak gap of the redox potential became wider (curve c) owing to the electronic repulsion between $Fe(CN)_6^{4-/3-}$ and the negative charges on the DNA backbones. After being blocked with MCH (curve d), the peak current decreased again. Additionally, the peak current in CV was further decreased, and the gap between the anodic and cathodic peaks became wider after the hybridization reaction between *c*DNA and *t*DNA (1 nM) (curve e). This phenomenon results from the fact that more negatively charged DNA strands were loaded on the electrode surface, hindering the diffusion of redox probe. However, the

DOI: 10.1021/acs.analchem.5b02395
Anal. Chem. XXXX, XXX, XXX−XXX

peak current increased correspondingly, and the peak gap of the redox potential became narrow (curve f) compared with the previous step.

Figure 3B shows the impedance spectra for the construction process of the DNA biosensor. The inset in Figure 3B represents the experimentally fitted Randles circuit parameters corresponding to the following four elements: the ohmic resistance of the solution (R_s); the charge-transfer resistance (R_{ct}), which represents the difficulty of electron transfer of a ferricyanide-redox probe between the solution and the electrode; the Warburg impedance (Z_w), resulting from the diffusion of ions from the bulk solution to the electrode interface; the interfacial double layer capacitance (C_{dl}) between the electrode and the solution, related to the surface condition of the electrode. This equivalent circuit model has been modified by a constant phase element (CPE) to replace the classical capacitance accounting for the inhomogeneity of the films on the electrode surface. As shown, the impedance spectrum of the AuNPs-modified GCE (curve b) exhibited a lower R_{ct} compared with the bare electrode (curve a). Afterward, the diameter of the semicircles increased successively with sequential assembly of *c*DNA (curve c), MCH (curve d), and *t*DNA (curve e), showing the gradual increase of R_{ct}. Nevertheless, the R_{ct} value decreased again correspondingly after hybridization with *r*DNA-grafted ZrHCF MNPs (curve f). Meanwhile, as shown in Figure S2, the order of the R_{ct} value is Fe_3O_4 MBs > ZrHCF MNPs > ZrHCF, demonstrating that ZrHCF can significantly improve the electron transfer ability of the modified electrode. These results are consistent with those of CVs, suggesting the successful fabrication of the electrochemical biosensor and providing a sensitive sensing platform for DNA detection.

Mechanism of Electrochemical DNA Assay. The electrochemical strategy is mainly based on ZrHCF MNPs as the signal nanoprobe for electrocatalytic H_2O_2 reduction. The electrochemical activity of the MBs, ZrHCF, and ZrHCF MNPs toward the H_2O_2 reduction was investigated by cyclic voltammetry ranging from −0.2 to 0.6 V with the scan rate of 50 mV s^{-1} in 0.1 M KCl aqueous solution. Figure 4 shows the CVs of the (A) GCE/MBs, (B) GCE/ZrHCF, and (C) GCE/ZrHCF MNPs in the absence (curve a) and presence (curve b) of 1.0 mM H_2O_2. The CVs of the GCE/MBs exhibit no electroactive response for H_2O_2 (Figure 4A). As for the case of GCE/ZrHCF (Figure 4B), the CV of GCE/ZrHCF shows a well-defined redox peak at around 0.2 V vs SCE owing to a single electron process of hexacyanoferrate (III/II) in the film.[41] Upon the addition of 1.0 mM H_2O_2, the cathodic peak currents of GCE/ZrHCF MNPs increase greatly (Figure 4C), indicating ZrHCF MNPs possess enhanced electrocatalytic activity to H_2O_2 compared to ZrHCF, attributed to the higher surface-to-volume ratio.[42] Furthermore, because of the electrocatalytic reduction potential of H_2O_2 at around 0.2 V, the dissolved oxygen has no interference to the detection signal.

It is worth noting that the coordination interaction between the ZrHCF MNPs and the poly(dG) spacers of *r*DNA has a paramount influence on the proposed electrochemical DNA sensor. Figure 5A shows the DPV responses of the proposed biosensor incubated with 1 nM target DNA for different *r*DNA-grafted ZrHCF MNPs in an electrolyte of 0.1 M KCl containing 1 mM H_2O_2: (a) *r*DNA1-grafted ZrHCF MNPs; (b) *r*DNA2-grafted ZrHCF MNPs. Obviously, it manifests a stronger response signal by using the *r*DNA-grafted ZrHCF MNPs with the poly(dG) spacer (curve a) in contrast with

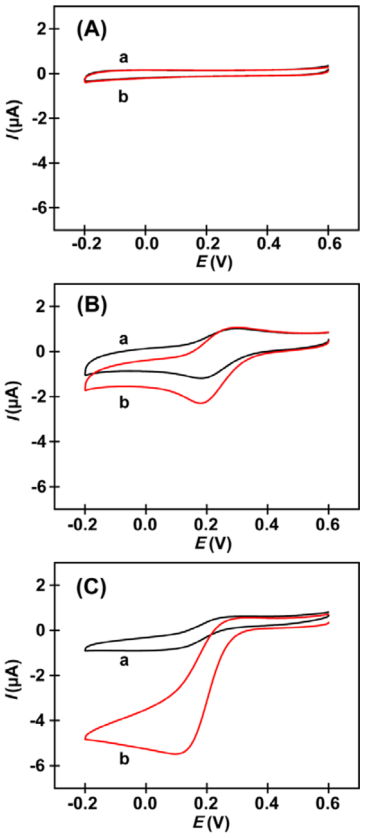

Figure 4. CVs recorded in 0.1 M KCl aqueous solution in the absence (a) and presence (b) of 1 mM H_2O_2 for (A) GCE/Fe_3O_4 MBs, (B) GCE/ZrHCF, and (C) GCE/ZrHCF MNPs; scan rate: 50 mV s^{-1}.

another no containing poly(dG) spacer in the 5′ terminal of *r*DNA (curve b), and the current signal is about 9.5 times of the latter, respectively. Bujoli and co-workers[24,43,44] have reported that *ss*DNA probes containing a poly(dG) spacer can be effectively assembled on the zirconium phosphonate modified surfaces, because the poly(dG) spacer may hold together the probe DNA, raising the avidity of the complex for terminal phosphate binding to the surface relative to a single strand. Specifically, the highest coordination number of Zr (IV) can reach 8, suggesting Zr (IV) on the shell ZrHCF frame compound can still be coordinated with phosphate groups from 5′-poly(dG) terminal of *r*DNA. Similarly, the *r*DNA with the 5′ terminal poly(dG) spacer has the ability to binding to the shell ZrHCF frame. Moreover, Bujoli and co-workers have introduced the idea of attaching protein probes onto a zirconium phosphonate surface via"zirconium−(OPO_3-peptide)" covalent bonds.[23] Of course, the single-stranded DNA can be firmly assembled on the ZrHCF MNPs by the "zirconium−(OPO_3-poly(dG) DNA)" covalent bonds to maintain DNA 5′ terminal-oriented (Figure 5B). Consequently, instead of some functional groups chemical modified in the terminal of DNA, the *r*DNA-grafted ZrHCF MNPs can be simply enriched, separated, and obtained just depending on the strong ligation between the 5′-polyG terminal of *r*DNA and Zr (IV) on the shell ZrHCF frame compound in the magnetic field. Furthermore, this strategy can also ensure the hybridization reaction efficiently between the target DNA and *r*DNA-grafted ZrHCF MNPs and the electrocatalytic ability of H_2O_2 reduction to achieve a highly sensitive detection for DNA successfully.

DOI: 10.1021/acs.analchem.5b02395
Anal. Chem. XXXX, XXX, XXX−XXX

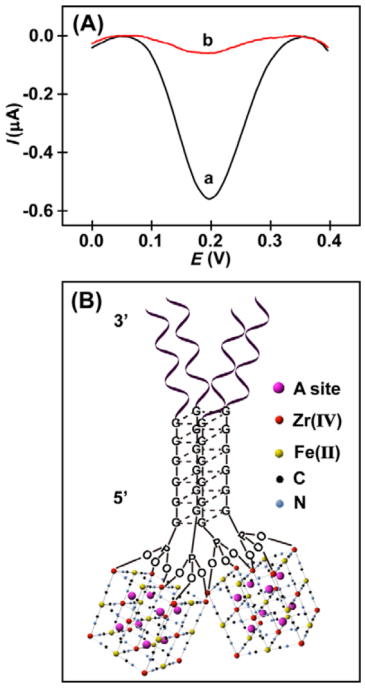

Figure 5. (A) DPV responses of the proposed biosensor incubated with 1 nM target DNA for different *r*DNA-grafted ZrHCF MNPs in an electrolyte of 0.1 M KCl containing 1 mM H_2O_2: (a) *r*DNA1-grafted ZrHCF MNPs; (b) *r*DNA2-grafted ZrHCF MNPs. DPV conditions: Pulse amplitude, 50 mV; sample width, 20 ms; pulse width, 200 ms; pulse period, 500 ms; quiet time, 2 s. (B) Illustration of the coordination between 5′-poly(dG) spacer terminal of *r*DNA and ZrHCF MNPs surface.

Optimization of Detection Conditions. First of all, considering whether it could achieve reasonable results by using the magnetic electrodes as the substrate of the DNA assay, the DPV responses between the conventional GCE (Figure S3A) and the MGCE (Figure S3B) were compared, respectively. The ΔI ($I - I_0$) for GCE and MGCE is −0.44 and −0.37 μA, respectively, where I_0 and I are the DPV peak currents of the biosensor before and after hybridization with the target DNA. Obviously, the background current signal is larger for MGCE due to the stronger physical adsorption of ZrHCF MNPs. Thus, it is more simple and convenient for the proposed DNA sensor to employ the conventional GCE as the substrate. Then, in order to achieve excellent electrochemical performance for the sensitive DNA assay, several experimental parameters were optimized, such as H_2O_2 concentration, the capture DNA concentration, and the hybridization time of capture DNA, target DNA, and *r*DNA-grafted ZrHCF MNPs (Figure 6). Since the electrolyte concentration has a momentous influence on the performance of biosensor, the reduction peak current was estimated at different H_2O_2 concentrations (Figure 6A). The reduction peak current was enhanced with a H_2O_2 concentration up to 1.0 mM and then tended to a plateau with further addition of H_2O_2, attributed to the electrocatalytic reduction of H_2O_2 being nearly saturated. Therefore, 1.0 mM of H_2O_2 was selected as the optimal concentration.

In addition, the surface density of *c*DNA immobilized on the modified electrode greatly influenced the sensitivity of electrochemical performance (Figure 6B).[45] The reduction peak current increased correspondingly in the range of 0−2.0 μM and gradually declined with further addition of *c*DNA. It suggests that a high surface density of *c*DNA could reduce the

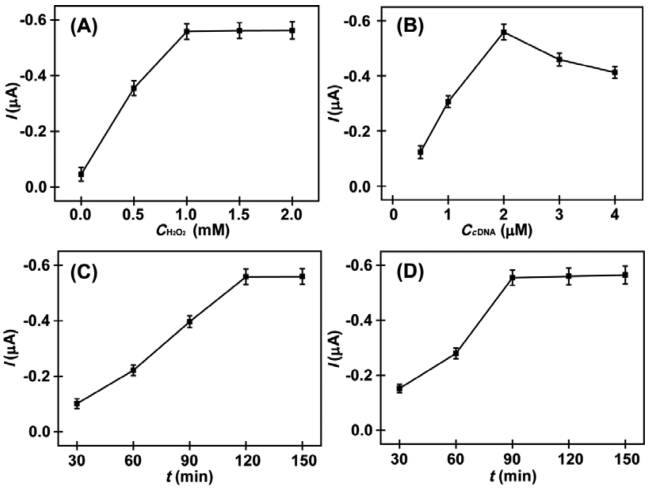

Figure 6. Effects of (A) H_2O_2 concentration, (B) *c*DNA concentration, (C) hybridization time of *c*DNA and *t*DNA, and (D) hybridization time of *r*DNA-grafted ZrHCF MNPs on DPV peak current responses of the biosensor. When one parameter changes, the others are under their optimal conditions. Error bars, SD, n = 3.

DNA hybridization efficiency, caused by steric hindrance.[46] To obtain high sensitivity, 2.0 μM was selected for the subsequent experiments.

The incubation time was another significant parameter affecting the analytical performance of the electrochemical biosensor. As shown in Figure 6C, when the hybridization time of *c*DNA and *t*DNA was increased, the reduction peak current was enhanced and then achieved a plateau after 120 min, indicating the hybridization reaction nearly reached the maximum. Thus, 120 min was employed for the optimal time of hybridization. Furthermore, Figure 6D displays the effect of the hybridization time of *t*DNA and *r*DNA-grafted ZrHCF MNPs on the reduction peak current response. When the incubation time was more than 90 min, no obvious reduction peak current increase was observed, demonstrating this time was sufficient for *t*DNA. Consequently, 90 min was selected as the optimal reaction time.

DNA Assay Performance. Figure 7A showed the DPVs of the proposed electrochemical sensor measured at various concentrations of DNA under the optimal experimental conditions. It is seen that the electrochemical signal increases with the increasing concentrations of target DNA. The calibration plot for the quantitative detection of *t*DNA is illustrated in Figure 7B. The reduction peak current was

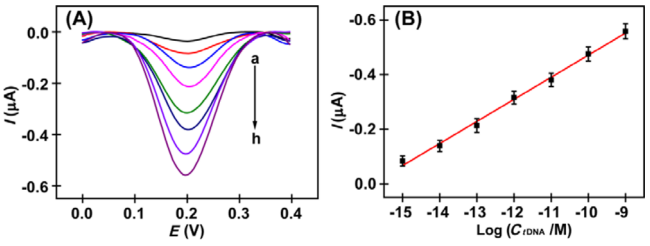

Figure 7. (A) DPV responses of the DNA biosensor incubated with different concentrations of tDNA in 0.1 M KCl solution containing 1 mM H_2O_2: (a) 0 fM, (b) 1 fM, (c) 10 fM, (d) 100 fM, (e) 1 pM, (f) 10 pM, (g) 100 pM, and (h) 1 nM. (B) The calibration plots of DPV peak current versus the logarithm of *t*DNA concentration. Error bars, SD, n = 3.

DOI: 10.1021/acs.analchem.5b02395
Anal. Chem. XXXX, XXX, XXX−XXX

proportional to the logarithm value of the *t*DNA concentration in a range of 1 fM to 1 nM. The regression equation was I (μA) = −1.275 − 0.081 log C (M) with a correlation coefficient of 0.996. The detection limit was estimated to be 0.43 fM. The analytical methods and the key performance characteristics of different DNA sensors are compared; the results were summarized in Table 1. As shown, this excellent analytical performance can be attributed to the good catalytic activity of the core−shell ZrHCF MNPs and the DNA with 5′ terminal poly(dG) spacer assembly on the ZrHCF MNPs. The wide enough linear range and lower detection limit can meet actual detection needs and, then, may develop nucleic acid detection sensors for clinical diagnosis. Meanwhile, the selectivity of proposed biosensor was evaluated by comparing the peak current changes toward different DNA sequences, such as *t*DNA, *sm*DNA, and *tm*DNA (Figure 8). The peak current of complete complementary *t*DNA was 5.2- and 6.9-fold higher than that of *sm*DNA and *tm*DNA, respectively. These results indicate the biosensor has excellent selectivity for target DNA against base mismatched sequences. Moreover, the DNA biosensor exhibits acceptable precision and reproducibility, with a relative standard deviation of 2.8% for five independent electrodes. Meanwhile, DPV responses of the biosensor have no obvious change after storage at 4 °C for half of a month, showing satisfactory stability.

Table 1. Comparison of the Performance of Our Proposed Sensor with Other Published DNA Sensors

analytical method[a]	linear range	detection limit	ref
FRET		5 pM	47
ECL	1.0 fM to 100 pM	0.37 fM	48
SPR	up to 10 nM	≈0.5 fM	49
EIS	1 pM to 500 nM	1 pM	50
SERS	10 pM to 10 nM	10 pM	51
PEC (HCR signal amplification)	25 fM to 100 pM	9.0 fM	52
DPV	10 fM to 10 nM	0.48 fM	6
DPV	1 fM to 1 nM	0.43 fM	this work

[a]FERT, fluorescence resonance energy transfer; ECL, electrochemiluminescence; SPR, surface plasma resonance; SERS, surface-enhanced Raman scattering; PEC, photoelectrochemical; HCR, hybridization chain reaction.

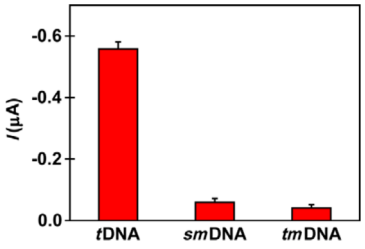

Figure 8. DPV peak current changes of the proposed biosensor at 1 nM *t*DNA, *sm*DNA, and *tm*DNA. Error bars, SD, n = 3.

Application in Biological Samples. To evaluate the proposed sensors' general applicability in biological samples analysis, recovery experiments were performed by adding 10 nM target DNA solution into 10% (v/v) diluted healthy human serum; the recovery and the RSD were calculated to be 97.3% and 2.05%, respectively, indicating the proposed DNA sensor was feasible for determination in real biological samples.

CONCLUSIONS

In summary, we have developed a new type of ZrHCF MNPs as signal label for the highly specific electrochemical DNA biosensor. The ZrHCF MNPs exhibit the following prominent characteristics: (1) The ZrHCF MNPs with core−shell structure possess favorable superparamagnetic properties. (2) The ZrHCF MNPs exhibit intrinsically enhanced peroxidase-like catalytic activity toward H_2O_2 reduction at about 0.2 V, and the dissolved oxygen has no interference to the catalytic reaction system. (3) The *r*DNA-grafted ZrHCF MNPs can be easily obtained by utilizing the bonding interaction of the Zr (IV) of the shell ZrHCF framework and the phosphate groups from the 5′-poly(dG) terminal of *r*DNA in the magnetic field. Taking full use of these advantages, we have further demonstrated the utilization of ZrHCF MNPs as signal-amplifying nanoprobes for an ultrasensitive electrochemical DNA array. This electrochemical approach may also provide a powerful tool to construct sensitive biosensing strategies with the multifunctional nanoprobes in bioanalysis.

ASSOCIATED CONTENT

Supporting Information

The Supporting Information is available free of charge on the ACS Publications website at DOI: 10.1021/acs.analchem.5b02395.

Figures of XPS response, EIS, and DPV responses (PDF)

AUTHOR INFORMATION

Corresponding Author

*Phone/Fax: +86-25-84303107. E-mail: danshan@njust.edu.cn; danshan@yzu.edu.cn.

Notes

The authors declare no competing financial interest.

ACKNOWLEDGMENTS

This research was supported by National Natural Science Foundation of China (Grant Nos. 21175114, 21305067), the Natural Science Foundation of Jiangsu Province (BK20130754), Ph.D. Fund of MOE for Young Teachers (0133219120019), Qing Lan project of Jiangsu Province, the Fundamental Research Funds for the Central Universities (30915015101, 30920130112012, 30920140112009), and a project founded by the priority academic program development of Jiangsu Higher Education Institutions.

REFERENCES

(1) Cibulskis, K.; Lawrence, M. S.; Carter, S. L.; Sivachenko, A.; Jaffe, D.; Sougnez, C.; Gabriel, S.; Meyerson, M.; Lander, E. S.; Getz, G. *Nat. Biotechnol.* **2013**, *31*, 213−219.

(2) Pattanayak, V.; Lin, S.; Guilinger, J. P.; Ma, E.; Doudna, J. A.; Liu, D. R. *Nat. Biotechnol.* **2013**, *31*, 839−843.

(3) Liang, Z.; Keeley, A. *Environ. Sci. Technol.* **2013**, *47*, 9324−9331.

(4) Abdalhai, M. H.; Maximiano Fernandes, A. n.; Bashari, M.; Ji, J.; He, Q.; Sun, X. *J. Agric. Food Chem.* **2014**, *62*, 12659−12667.

(5) Drummond, T. G.; Hill, M. G.; Barton, J. K. *Nat. Biotechnol.* **2003**, *21*, 1192−1199.

(6) Ling, P.; Lei, J.; Zhang, L.; Ju, H. *Anal. Chem.* **2015**, *87*, 3957−3963.

(7) Xiao, Y.; Qu, X.; Plaxco, K. W.; Heeger, A. J. *J. Am. Chem. Soc.* **2007**, *129*, 11896−11897.

DOI: 10.1021/acs.analchem.5b02395
Anal. Chem. XXXX, XXX, XXX−XXX

(8) Hu, J.; Yu, Y.; Brooks, J. C.; Godwin, L. A.; Somasundaram, S.; Torabinejad, F.; Kim, J.; Shannon, C.; Easley, C. J. *J. Am. Chem. Soc.* **2014**, *136*, 8467−8474.
(9) Munge, B.; Liu, G.; Collins, G.; Wang, J. *Anal. Chem.* **2005**, *77*, 4662−4666.
(10) Miranda-Castro, R.; de-los-Santos-Álvarez, P.; Lobo-Castañón, M. J.; Miranda-Ordieres, A. J.; Tuñón-Blanco, P. *Anal. Chem.* **2007**, *79*, 4050−4055.
(11) Reddy, L. H.; Arias, J. L.; Nicolas, J.; Couvreur, P. *Chem. Rev.* **2012**, *112*, 5818−5878.
(12) Fojta, M.; Havran, L.; Vojtiskova, M.; Palecek, E. *J. Am. Chem. Soc.* **2004**, *126*, 6532−6533.
(13) Lee, I. S.; Lee, N.; Park, J.; Kim, B. H.; Yi, Y.-W.; Kim, T.; Kim, T. K.; Lee, I. H.; Paik, S. R.; Hyeon, T. *J. Am. Chem. Soc.* **2006**, *128*, 10658−10659.
(14) Acharya, G.; Chang, C.-L.; Doorneweerd, D. D.; Vlashi, E.; Henne, W. A.; Hartmann, L. C.; Low, P. S.; Savran, C. A. *J. Am. Chem. Soc.* **2007**, *129*, 15824−15829.
(15) Hill, H. D.; Mirkin, C. A. *Nat. Protoc.* **2006**, *1*, 324−336.
(16) Urbanova, V.; Magro, M.; Gedanken, A.; Baratella, D.; Vianello, F.; Zboril, R. *Chem. Mater.* **2014**, *26*, 6653−6673.
(17) Tang, D.; Yuan, R.; Chai, Y. *Anal. Chem.* **2008**, *80*, 1582−1588.
(18) Zheng, T.; Zhang, Q.; Feng, S.; Zhu, J.-J.; Wang, Q.; Wang, H. *J. Am. Chem. Soc.* **2014**, *136*, 2288−2291.
(19) Sitnikova, N. A.; Komkova, M. A.; Khomyakova, I. V.; Karyakina, E. E.; Karyakin, A. A. *Anal. Chem.* **2014**, *86*, 4131−4134.
(20) Fiorito, P. A.; Gonçales, V. R.; Ponzio, E. A.; de Torresi, S. I. C. *Chem. Commun.* **2005**, 366−368.
(21) Queffélec, C.; Petit, M.; Janvier, P.; Knight, D. A.; Bruno, B. *Chem. Rev.* **2012**, *112*, 3777−3807.
(22) Wang, Q.; Zhong, L.; Sun, J.; Shen. *Chem. Mater.* **2005**, *17*, 3563−3569.
(23) Liu, H.; Queffélec, C.; Charlier, C.; Defontaine, A.; Fateh, A.; Tellier, C.; Talham, D. R.; Bujoli, B. *Langmuir* **2014**, *30*, 13949−13955.
(24) Nonglaton, G.; Benitez, I. O.; Guisle, I.; Pipelier, M.; Léger, J.; Dubreuil, D.; Tellier, C.; Talham, D. R.; Bujoli, B. *J. Am. Chem. Soc.* **2004**, *126*, 1497−1502.
(25) Zhou, H.; Ye, M.; Dong, J.; Corradini, E.; Cristobal, A.; Heck, A. J.; Zou, H.; Mohammed, S. *Nat. Protoc.* **2013**, *8*, 461−480.
(26) Meng, H.-M.; Fu, T.; Zhang, X.-B.; Wang, N.-N.; Tan, W.; Shen, G.-L.; Yu, R.-Q. *Anal. Chem.* **2012**, *84*, 2124−2128.
(27) Wang, Z.; Sun, N.; He, Y.; Liu, Y.; Li, J. *Anal. Chem.* **2014**, *86*, 6153−6159.
(28) Ma, W.-F.; Zhang, C.; Zhang, Y.-T.; Yu, M.; Guo, J.; Zhang, Y.; Lu, H.-J.; Wang, C.-C. *Langmuir* **2014**, *30*, 6602−6611.
(29) Zhao, M.; Deng, C.; Zhang, X. *Chem. Commun.* **2014**, *50*, 6228−6231.
(30) Zhu, X.; Li, B.; Yang, J.; Li, Y.; Zhao, W.; Shi, J.; Gu, J. *ACS Appl. Mater. Interfaces* **2015**, *7*, 223−231.
(31) Della Giustina, G.; Zambon, A.; Lamberti, F.; Elvassore, N.; Brusatin, G. *ACS Appl. Mater. Interfaces* **2015**, *7*, 13280−13288.
(32) Dong, J. X.; Li, N. B.; Luo, H. Q. *Anal. Methods* **2013**, *5*, 5541.
(33) Mahmoud, M.; El-Sayed, M. *J. Phys. Chem. C* **2007**, *111*, 17180−17183.
(34) Ding, Y.; Hu, Y.-L.; Gu, G.; Xia, X.-H. *J. Phys. Chem. C* **2009**, *113*, 14838−14843.
(35) Ding, Y.; Hu, Y.; Zhang, L.; Chen, Y.; Jiang, X. *Biomacromolecules* **2006**, *7*, 1766−1772.
(36) Feng, L.-D.; Gu, M.-M.; Yang, Y.-L.; Liang, G.-X.; Zhang, J.-R.; Zhu, J.-J. *J. Phys. Chem. C* **2009**, *113*, 8743−8749.
(37) Wood, M. H.; Welbourn, R. J.; Charlton, T.; Zarbakhsh, A.; Casford, M. T.; Clarke, S. M. *Langmuir* **2013**, *29*, 13735−13742.
(38) Zhang, M.; Yu, P.; Mao, L. *Acc. Chem. Res.* **2012**, *45*, 533−543.
(39) Li, W.; Yuan, R.; Chai, Y. *J. Phys. Chem. C* **2010**, *114*, 21397−21404.
(40) Tong, S.; Ren, B.; Zheng, Z.; Shen, H.; Bao, G. *ACS Nano* **2013**, *7*, 5142−5150.
(41) Byrd, H.; Chapman, B. E.; Talley, C. L. *J. Chem. Educ.* **2013**, *90*, 775−777.
(42) Asakura, D.; Li, C. H.; Mizuno, Y.; Okubo, M.; Zhou, H.; Talham, D. R. *J. Am. Chem. Soc.* **2013**, *135*, 2793−2799.
(43) Monot, J.; Petit, M.; Lane, S. M.; Guisle, I.; Léger, J.; Tellier, C.; Talham, D. R.; Bujoli, B. *J. Am. Chem. Soc.* **2008**, *130*, 6243−6251.
(44) Lane, S. M.; Monot, J.; Petit, M.; Tellier, C.; Bujoli, B.; Talham, D. R. *Langmuir* **2008**, *24*, 7394−7399.
(45) Southern, E.; Mir, K.; Shchepinov, M. *Nat. Genet.* **1999**, *21*, 5−9.
(46) Zhang, J.; Song, S.; Zhang, L.; Wang, L.; Wu, H.; Pan, D.; Fan, C. *J. Am. Chem. Soc.* **2006**, *128*, 8575−8580.
(47) Alonso-Cristobal, P.; Vilela, P.; El-Sagheer, A.; Lopez-Cabarcos, E.; Brown, T.; Muskens, O.; Rubio-Retama, J.; Kanaras, A. *ACS Appl. Mater. Interfaces* **2015**, *7*, 12422−12429.
(48) Deng, S.; Yuan, P.; Ji, X.; Shan, D.; Zhang, X. *ACS Appl. Mater. Interfaces* **2015**, *7*, 543−552.
(49) Zagorodko, O.; Spadavecchia, J.; Serrano, A. Y.; Larroulet, I.; Pesquera, A.; Zurutuza, A.; Boukherroub, R.; Szunerits, S. *Anal. Chem.* **2014**, *86*, 11211−11216.
(50) Yang, Y.; Li, C.; Yin, L.; Liu, M.; Wang, Z.; Shu, Y.; Li, G. *ACS Appl. Mater. Interfaces* **2014**, *6*, 7579−7584.
(51) Kang, T.; Yoo, S. M.; Yoon, I.; Lee, S. Y.; Kim, B. *Nano Lett.* **2010**, *10*, 1189−1193.
(52) Li, C.; Wang, H.; Shen, J.; Tang, B. *Anal. Chem.* **2015**, *87*, 4283−4291.

DOI: 10.1021/acs.analchem.5b02395
Anal. Chem. XXXX, XXX, XXX−XXX